Diffuse approximation for identification of the mechanical properties of microcapsules

Carlos Quesada, Claire Dupont, Pierre Villon, Anne-Virginie Salsac

Diffuse approximation for the identification of the mechanical properties of microcapsules

Journal Title
XX(X):1–8

DOI: 10.1177/ToBeAssigned
www.sagepub.com/
SAGE

Carlos Quesada[1] and Claire Dupont[1] and Pierre Villon[2] and Anne-Virginie Salsac [1]

Abstract

A novel data-driven real-time procedure based on diffuse approximation is proposed to characterize the mechanical behavior of liquid-core microcapsules from their deformed shape and identify the mechanical properties of the sub-micron-thick membrane that protects the inner core through inverse analysis. The method first consists of experimentally acquiring the deformed shape that a given microcapsule takes at steady-state when it flows through a microfluidic microchannel of comparable cross-sectional size. From the mid-plane capsule profile, we deduce two characteristic geometrical quantities that uniquely characterize the shape taken by the microcapsule under the external hydrodynamic stresses. To identify the value of the unknown rigidity of the membrane and the size of the capsule, we compare the geometrical quantities to the values predicted numerically using a fluid-structure-interaction model by solving the three-dimensional capsule-flow interactions. The complete numerical data set is obtained off-line by systematically varying the governing parameters of the problem, i.e. the capsule-to-tube confinement ratio and the capillary number, ratio of the viscous to elastic forces. We show that diffuse approximation efficiently estimates the unknown mechanical resistance of the capsule membrane. We validate the data-driven procedure by applying it to the geometrical and mechanical characterization of ovalbumin microcapsules (diameter of the order of a few tens of microns). As soon as the capsule is sufficiently deformed to exhibit a parachute shape at the rear, the capsule size and surface shear modulus are determined with an error of only 0.2% and 2.7%, respectively, as compared to 2-3% and 25% without it, in the best cases (Hu *et al.* PRE 2013). Diffuse approximation thus allows to quasi-instantly provide the capsule size and resistance with a very high precision. It opens interesting perspectives for all the industrial applications that require a tight control of the capsule mechanical properties in order to secure their behavior when they transport active material.

Keywords

Identification, mechanical properties, microcapsules, data-driven method, diffuse approximation

Introduction

A capsule is a liquid droplet enclosed within a thin elastic membrane. Capsules are found in nature in the form of cells or eggs, but they can also be artificially synthesized for multiple industrial and clinical purposes (1; 2). The pharmaceutical (3), textile (4), cosmetic (5) and food industries (6) make a wide use of artificial capsules to control the release of active ingredients (drugs, cells, viruses, ...), aromas or flavors. The capsule radius is typically micrometric, ranging from a few microns to a few tens of microns.

Whether natural or artificial, capsules are always in suspension in an external fluid, which subjects the capsules to hydrodynamic forces when it flows and leads to their deformation. The dynamic behavior of capsules is thus governed by three-dimensional fluid-structure interactions, in which the membrane plays a crucial role. It ensures the protection and transport of the internal content, the control of its potential release and the deformability of the capsule thanks to its thinness and elastic resistance. However, the small size and fragility of the microcapsule make the assessment of its mechanical properties a challenging task. Different experimental methods exist to deform micrometric capsules and estimate the mechanical properties. For individual cells and vesicles, micropipette aspiration is the most used technique (7). The mechanical properties are obtained by aspirating the particle into a micropipette at different pressure conditions and measuring the resulting deformation. Atomic Force Microscopy (AFM) can also be used to deform capsules under known forces (8). For capsule populations in suspension, more recent techniques have been developed based on microfluidic experiments. They consist in flowing the capsules through a microchannel in order to apply inverse analysis techniques to the observed deformed profiles (9; 10; 11).

In all the cases, a numerical model is needed to determine the values of the mechanical properties. For the microfluidic experiments, numerical simulations based on the resolution of complex fluid-structure interactions (12; 13; 14) provide the deformed profile of the capsules at steady-state. However,

[1]Biomechanics and Bioengineering Laboratory (UMR 7338), CNRS - Université de Technologie de Compiègne, Compiègne, France
[2]Roberval Laboratory, Université de Technologie de Compiègne, Compiègne, France

Corresponding author:
Anne-Virginie Salsac Biomechanics and Bioengineering Laboratory (UMR 7338), CNRS - Université de Technologie de Compiègne, CS 60319, 60203 Compiègne, France
Email: a.salsac@utc.fr

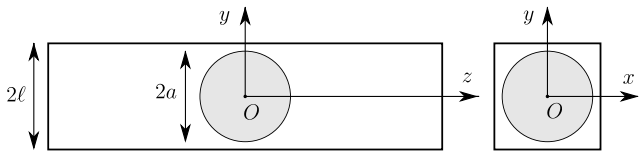

Figure 1. Initial configuration of a spherical capsule of radius a in a square-section microchannel of side 2ℓ. Longitudinal and cross-sectional views.

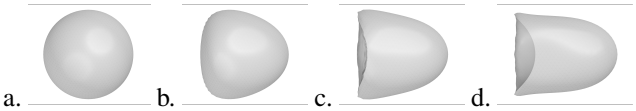

Figure 2. Numerical simulation of the evolution of a capsule, from rest to steady-state, as it flows along the microchannel. The capsule is shown for $Ca = 0.12$ and $a/\ell = 0.9$ at the non-dimensional times $Ut/\ell = 0$ (a), 0.2 (b), 0.6 (c) and 2.4 (d).

identifying the mechanical properties of a capsule by comparing its deformation with those obtained in the numerical simulations remains challenging. None of the existing studies proposed a consistent method to solve the inverse problem.

In this work, we present a fast, accurate, self-contained technique for inverse analysis using a data-driven method based on the diffuse approximation (15). We focus on experimental data obtained by flowing a microcapsule in microfluidic square-section channel of comparable size. The experimental data consists of the capsule velocity and mid-plane profile at steady-state, from which we deduce geometrical quantities (e.g. maximum extension length and axial length) that are characteristic of it. Numerical models of this exact problem exist (16; 13). The one by Hu *et al.* (13) is used off-line to get a complete numerical data-set of the three-dimensional steady-state shapes adopted by the capsule inside the microchannel for a wide range of values of the input parameters: the size ratio, which corresponds to the capsule-to-tube confinement ratio, and the capillary number, ratio of the viscous friction force acting onto the capsule to the restoring membrane elastic force. A database of two-dimensional capsule contours (cross-cuts) is obtained from these numerical simulations along with their geometrical quantities. The algorithm used to identify the mechanical properties of the capsules consists of applying the diffuse approximation method to the numerical database to deduce the size ratio and capillary number that correspond to the measured values of the geometrical parameters of the capsule profile.

Materials and methods

Problem description

We consider an initially spherical capsule of radius a flowing within a long prismatic microchannel with constant square cross-section of side 2ℓ (Fig. 1). The thin membrane of the capsule is made of an impermeable hyperelastic isotropic material with surface shear modulus G_S. As the capsule flows, the hydrodynamic forces inside the channel gradually deform its membrane (Fig. 2). Eventually, the capsule reaches a steady-state shape that is function of

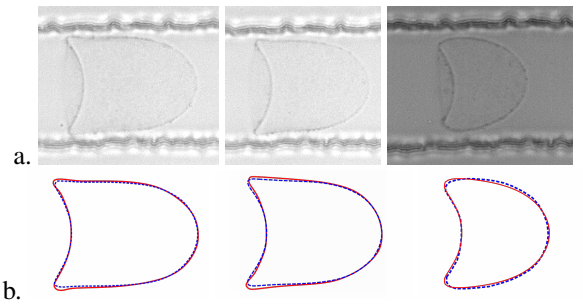

Figure 3. (a) Experimental images of ovalbumin microcapsules flowing at steady-state (10). (b) In red, their corresponding contours captured using *ImageJ*; in dashed blue, the contour identified by diffuse approximation: $Ca = 0.064$ and $a/\ell = 1.02$ (left); $Ca = 0.082$ and $a/\ell = 0.96$ (center); and $Ca = 0.012$ and $a/\ell = 0.75$ (right).

the constitutive law of the membrane and two independent parameters:

- The capillary number Ca, defined as

$$Ca = \mu U / G_S, \tag{1}$$

  where μ is the viscosity of the external liquid and U is the mean axial velocity of the undisturbed Poiseuille flow.
- The size ratio a/ℓ between the capsule radius and the channel cross-dimension.

Our objective is to obtain the value of G_S, which is the mechanical property that governs the capsule membrane behavior.

Experimental procedure

A suspension of polydisperse ovalbumin microcapsules of average diameter equal to 50 μm and of submicronic membrane thickness is prepared as described in (17) and injected into a microfluidic system by means of a syringe pump at different flow rates. The microfluidic system consists of a straight channel of square section, 5 mm in length and $\ell \sim 50$ μm. It is fabricated in PDMS following the procedure provided in (18; 19). The motion and deformation of each capsule is observed with a microscope connected to a high-resolution high-speed camera. Two-dimensional side-view gray-scale images of capsules are obtained as they flow in the microchannel (Fig. 3a). More technical details on the experimental setup can be found in (9; 10).

The deformed profile of the capsules acquired experimentally can be characterized by geometrical quantities that we normalize using the channel characteristic size ℓ (Fig. 4). The inverse analysis algorithm proposed here requires the measurement of only two of those quantities:

- The maximum extension of the capsule along the longitudinal axis L_z/ℓ.
- The axial length L_a/ℓ.

Together, they provide the information on the depth of the parachute depth, $L_p = L_z - L_a$ (Fig. 4), which measures the concavity at the rear part of the capsule, and was shown to relate well with the global deformation of the capsule (20). It is, however, not appropriate to use it as one of the two

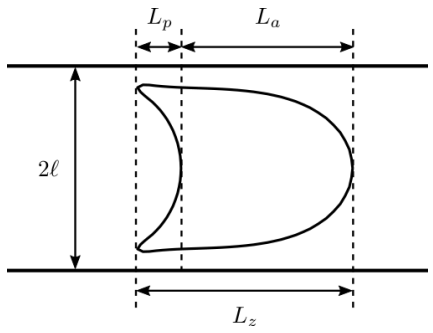

Figure 4. Some geometrical quantities that can be measured from the capsule deformed profile: the maximum extension L_z along the z-axis, the axial length L_a and the parachute depth $L_p = L_z - L_a$ (if any).

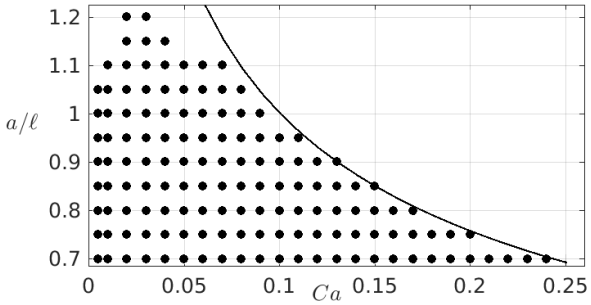

Figure 5. Values of Ca and a/ℓ included in the database. The domain where a steady-state capsule deformation exists is delimited by the black line in the case of capsules following the neo-Hookean constitutive law (21).

geometrical parameters, as the errors of its estimation are much larger than for L_z and L_a.

The other quantity obtained experimentally is the velocity of the center of mass of the capsule v_o. It is determined at steady-state by measuring the position of a specific point on the membrane on successive time frames. Three quantities are, however, unknown:

- The membrane surface shear modulus G_S.
- The capsule radius a, which greatly varies from one capsule of the suspension to the next.
- The mean undisturbed external flow velocity U, which is impossible to know with precision, since the flow rate provided by syringe pumps always fluctuate a little over time.

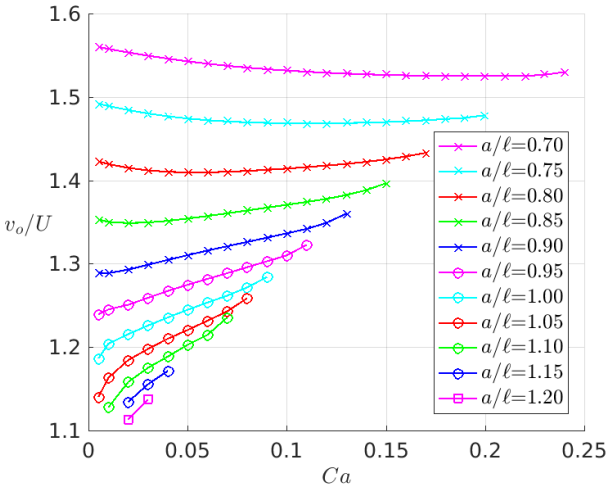

Figure 6. Values of v_o/U as a function of Ca and a/ℓ.

Equations governing the forward fluid-structure interaction problem

The inertialess flow of the deformable micrometric capsule along the channel is obtained by solving the Stokes equations in the external ($\beta = 1$) and internal fluids ($\beta = 2$), together with the membrane equilibrium equation. For the fluid problem, let $\boldsymbol{v}^{(\beta)}$, $\boldsymbol{\sigma}^{(\beta)}$ and $p^{(\beta)}$ be the velocity, stress and pressure fields in the two fluids, non-dimensionalized using ℓ as characteristic length, ℓ/U as characteristic time and $G_S\ell$ as characteristic force. The Stokes equations

$$\nabla p^{(\beta)} = Ca\nabla^2 \boldsymbol{v}^{(\beta)}, \quad \nabla \cdot \boldsymbol{v}^{(\beta)} = 0, \quad \beta = 1, 2. \tag{2}$$

are solved in the domain shown in Fig. 1, assuming no flow disturbance far from the capsule (i.e. the velocity field is the one in the absence of capsule at the inlet and outlet of the square channel), a no-slip boundary condition on the channel and capsule walls and the continuity of the normal load on the capsule wall:

$$(\boldsymbol{\sigma}^{(1)} - \boldsymbol{\sigma}^{(2)}) \cdot \boldsymbol{n} = \boldsymbol{q}, \tag{3}$$

where $\boldsymbol{n}$ is the unit normal vector pointing towards the external fluid and $\boldsymbol{q}$ is the non-dimensionalized external load per unit area exerted by the fluids on the membrane due to viscous traction. For the solid problem, let $\boldsymbol{\tau}$ be the non-dimensionalized Cauchy tension tensor, which corresponds to the forces per unit arclength in the plane of the membrane. The local equilibrium equation governing the inertialess membrane is then

$$\boldsymbol{\nabla}_s \cdot \boldsymbol{\tau} + \boldsymbol{q} = \boldsymbol{0}, \tag{4}$$

where $\boldsymbol{\nabla}_s \cdot$ is the surface divergence operator.

Numerical model

Eq. 2 and 4, along with the above boundary conditions, are solved with the numerical model described in (13). This model, hereafter referred to BI–FE model, couples the Boundary Integral method to solve the fluid flows with the Finite Element method to solve the membrane mechanics. It is used to obtain an extensive database of steady-state shapes of capsules in flow. The values of the parameters Ca and a/ℓ, as well as the constitutive law that governs the capsule membrane behavior, are the input parameters of the numerical model. The neo-Hookean law, whose strain-softening behavior under large deformation has proven to be appropriate to describe ovalbumin capsules (9), is presently considered to model the membrane. The deformed profile of the capsule at steady-state and the velocity ratio v_o/U are some of the outputs of the model.

A database of $M = 137$ three-dimensional steady-state deformed capsules has been generated using the numerical model. The different values of Ca and a/ℓ, for which the simulations have been computed, are shown in Fig. 5, and their associated values of v_o/U are represented in Fig. 6.

We shall call $\mathcal{T}$ the set of points $\boldsymbol{\theta}^i = \left(\theta_1^i, \theta_2^i, \theta_3^i\right)$, where the superscript i (for $i = 1 \dots M$) refers to the i-th capsule simulation, and where θ_1^i, θ_2^i and θ_3^i refer to its corresponding values of Ca, a/ℓ and v_o/U, respectively. The representation of the points of $\mathcal{T}$ in the θ-space shows that they all lie on a surface $\mathcal{S}_\mathcal{T}$ (Fig. 7). The contours of all the shapes in the plane $x = 0$ have then been obtained, for comparison with the experimental profiles. For each of them, the geometrical quantities of their deformed profiles have been computed and added to the database. We shall call $\mathcal{L}$ the set of points $\boldsymbol{\lambda}^i = \left(\lambda_1^i, \lambda_2^i\right)$, where the superscript i (for $i = 1 \dots M$) identically refers to the i-th capsule simulation, and where λ_1^i and λ_2^i refer to its corresponding values of L_z/ℓ and L_a/ℓ (Fig. 8a).

Inverse analysis approach

The inverse analysis method presented here characterizes the mechanical behavior of the capsule membrane by determining the value of its surface shear modulus G_S, as well as the capsule radius a and the external flow speed U, using two steps further described below. From the geometrical quantities measured experimentally (L_z/ℓ and L_a/ℓ) and with the help of the database computed using the BI–FE model, we first use a diffuse approximation technique to obtain the unknown values of the capillary number Ca and size ratio a/ℓ, which are the two independent parameters on which the capsule deformation depends. Knowing Ca and a/ℓ, we then determine the velocity ratio v_o/U by interpolating the numerical results of Fig. 7. The surface shear modulus G_S is finally deduced from the values of Ca and v_o/U using Eq. 1, since the velocity of the capsule center of mass v_o is estimated from the acquired images and the viscosity of the external liquid μ measured prior to conducting the experiments.

Diffuse approximation

Only the two independent parameters of the problem Ca and a/ℓ are considered when applying the diffuse approximation method. We shall call $\widehat{\mathcal{T}}$ the reduced set of points $\widehat{\boldsymbol{\theta}}^i = \left(\theta_1^i, \theta_2^i\right)$. From Fig. 8a, one can notice that the points of $\mathcal{L}$ are inclined. To apply diffuse approximation more easily, a rotation of -45° around the axis perpendicular to the plane defined by $\mathcal{L}$ and centered on (0,0) is applied. We shall call $\mathcal{L}'$ the set of points $\boldsymbol{\lambda'}^i$ (Fig. 8b). The points of $\widehat{\mathcal{T}}$ and $\mathcal{L}'$ define respectively the surfaces $\mathcal{S}_{\widehat{\mathcal{T}}}$ and $\mathcal{S}_{\mathcal{L}'}$. We deduce that any point not present in the database ($\boldsymbol{\lambda'} \notin \mathcal{L}'$) but lying on the surface $\mathcal{S}_{\mathcal{L}'}$ corresponds to admissible geometrical quantities that may be obtained experimentally (22).

Using diffuse approximation techniques (15), we map an arbitrary point $\boldsymbol{\lambda'} \notin \mathcal{L}'$ on the surface $\mathcal{S}_{\mathcal{L}'}$ to a corresponding point $\widehat{\boldsymbol{\theta}} \notin \widehat{\mathcal{T}}$ on the surface $\mathcal{S}_{\widehat{\mathcal{T}}}$. The idea is to use this mapping to estimate the unknown values of Ca and a/ℓ knowing the values of the experimentally measured geometrical quantities L_z'/ℓ and L_a'/ℓ. To achieve this, diffuse approximation makes use of a local weighted least squares fitting that is valid in a small neighborhood around $\boldsymbol{\lambda'}$ and is based on the points included within it (Fig. 9). Within this domain centered on $\boldsymbol{\lambda'}$, the coefficients λ_j' ($j = 1, 2$) can

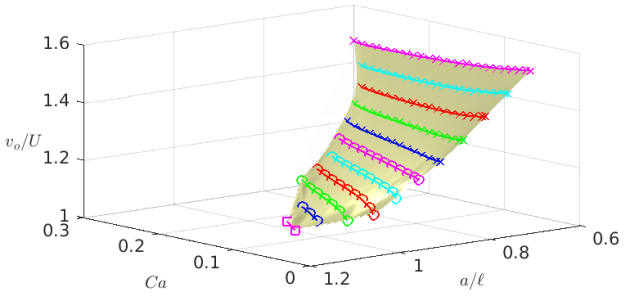

Figure 7. Points of $\mathcal{T}$ in the θ-space conforming the surface $\mathcal{S}_\mathcal{T}$.

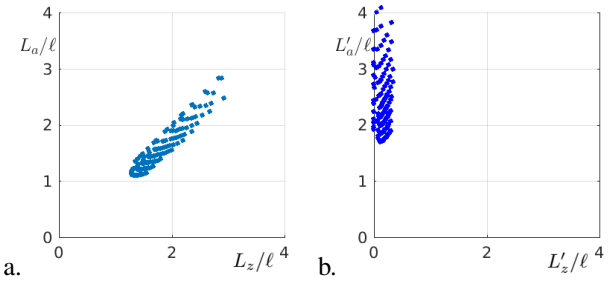

Figure 8. a. View of the points of $\mathcal{L}$ in the λ-space: they lie on a narrow, elongated and tilted surface $\mathcal{S}_\mathcal{L}$. b. To ease the application of the diffuse approximation technique, we apply a rotation of -45° around the axis perpendicular to the plane defined by $\mathcal{L}$ and centered on (0,0). L_z/ℓ and L_a/ℓ thus become L_z'/ℓ and L_a'/ℓ.

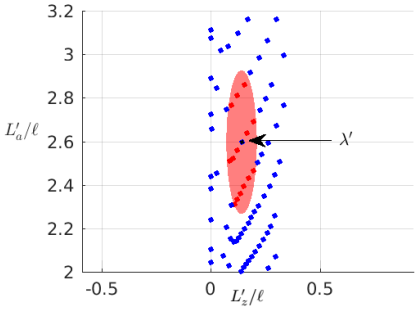

Figure 9. Region of the λ'-space showing an arbitrary point $\boldsymbol{\lambda'} \notin \mathcal{L}'$ and its elliptical neighborhood, which includes $N = 14$ points $\boldsymbol{\lambda'}^i \in \mathcal{L}'$.

be locally approximated by the expression

$$\lambda_j' = \boldsymbol{p}(\boldsymbol{\theta})^{\mathrm{T}} \boldsymbol{a}^j = \begin{bmatrix} 1 & \theta_1 & \theta_2 \end{bmatrix} \begin{bmatrix} a_0^j \\ a_1^j \\ a_2^j \end{bmatrix}, \qquad (5)$$

where $\boldsymbol{p}$ is a vector of independent polynomial functions and $\boldsymbol{a}^j$ are the approximation coefficient vectors.

To approximate $\boldsymbol{\lambda'}$, we weight the contribution of the points $\boldsymbol{\lambda'}^i$ ($i = 1 \dots M$), contained in the elliptical neighborhood, proportionally to the distance d between the points $\boldsymbol{\lambda'}^i$ and $\boldsymbol{\lambda'}$. Distances are computed as

$$d^i = \left(\sum_{j=1}^{2} \gamma_j \left(\lambda_j'^i - \lambda_j'\right)^2 \right)^{\frac{1}{2}}.$$

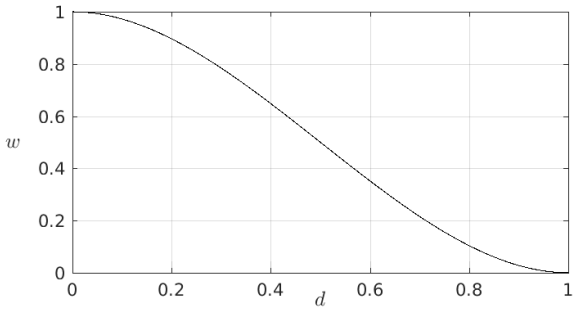

Figure 10. Weight function $w(d)$.

The parameters γ_j (for $j = 1, 2$) are equal to 1 in the case of a circular neighborhood, but in the present case, we used $\gamma_1 = 1$ and $\gamma_2 = 0.05$ to suit the elongated shape of the surface $\mathcal{S}_{\mathcal{L}}$ (Fig. 9).

The weight assigned to each $\boldsymbol{\lambda'}^i$ is chosen to be

$$w(D) = \begin{cases} 2D^3 - 3D^2 + 1, & \text{if } D \leq 1 \\ 0, & \text{otherwise} \end{cases},$$

where the normalized distance $D = d^i/\delta$ is 0 for a point in the center of the neighborhood ($d^i = 0$) and 1 for a point located at its boundary ($d^i = \delta$). The value of $w(D)$ ranges from 1 to 0, decreasing monotonically as D increases (Fig. 10). To ensure that the system of equations (see below) is not overdetermined, the neighborhood must include more points $\boldsymbol{\lambda'}^i \in \mathcal{L}'$ than the number of elements in vector $\boldsymbol{a}^j$ (i.e. $N > 3$ in this case). To meet this constraint, the neighborhood is chosen to have a variable size, but to keep its elliptical shape with fixed proportions in order to always include $N = 14$ points regardless the position of $\boldsymbol{\lambda'}$ in $\mathcal{S}_{L'}$. This is achieved by setting δ (the distance to the boundary of the neighborhood) as the N-th largest distance of d^i.

To find the vectors $\boldsymbol{a}^j$, diffuse approximation uses least squares to minimize the following function J:

$$J(\boldsymbol{a}^1, \boldsymbol{a}^2) = \frac{1}{2} \sum_{n=1}^{N} w(d_n) \left(\sum_{j=1}^{2} \left(\lambda_j'^n - \boldsymbol{p}(\widehat{\boldsymbol{\theta}}^n)^{\mathrm{T}} \boldsymbol{a}^j \right)^2 \right).$$

This results in

$$\boldsymbol{a}^j = \left(\boldsymbol{P}^{\mathrm{T}} \boldsymbol{W} \boldsymbol{P}\right)^{-1} \boldsymbol{P}^{\mathrm{T}} \boldsymbol{W} \boldsymbol{L'}_j,$$

where $\boldsymbol{P}$ is a $N \times 3$ matrix containing the vectors $\boldsymbol{p}$ of the N points included inside the neighborhood; $\boldsymbol{L'}^j$, for $j = 1, 2$, are two vectors containing the N values of λ'_j of the points in the neighborhood; and $\boldsymbol{W}$ is a $N \times N$ diagonal matrix with the values of the weights associated to each point in the neighborhood:

$$\boldsymbol{P} = \begin{bmatrix} \boldsymbol{p}(\boldsymbol{\theta}^1)^{\mathrm{T}} \\ \boldsymbol{p}(\boldsymbol{\theta}^2)^{\mathrm{T}} \\ \vdots \\ \boldsymbol{p}(\boldsymbol{\theta}^N)^{\mathrm{T}} \end{bmatrix}, \quad \boldsymbol{L'}^j = \begin{bmatrix} \lambda_j'^1 \\ \lambda_j'^2 \\ \vdots \\ \lambda_j'^N \end{bmatrix},$$

$$\boldsymbol{W} = \begin{bmatrix} w_1 & 0 & \cdots & 0 \\ 0 & w_2 & \cdots & 0 \\ \vdots & \vdots & \ddots & \vdots \\ 0 & 0 & \cdots & w_N \end{bmatrix}.$$

Once the vectors $\boldsymbol{a}^1$ and $\boldsymbol{a}^2$ are known, $\widehat{\boldsymbol{\theta}}$ can be computed by

$$\widehat{\boldsymbol{\theta}} = \boldsymbol{A}^{\dagger} \boldsymbol{X},$$

where

$$\boldsymbol{X} = \begin{bmatrix} \lambda'_1 - a_0^1 \\ \lambda'_2 - a_0^2 \end{bmatrix}, \quad \boldsymbol{A} = \begin{bmatrix} a_1^1 & a_2^1 \\ a_1^2 & a_2^2 \end{bmatrix}$$

and $\boldsymbol{A}^{\dagger}$ is the Moore-Penrose pseudoinverse of $\boldsymbol{A}$.

Interpolation

The diffuse approximation allows us to estimate the values of Ca and a/ℓ for any arbitrary point $\boldsymbol{\lambda'} \notin \mathcal{L}'$ but the quantity v_0/U remains unknown. To estimate it, we apply a Delaunay triangulation on $\mathcal{S}_{\mathcal{T}}$ and identify the triangle corresponding to $\widehat{\theta}$ by projecting it onto $\mathcal{S}_{\mathcal{T}}$. The velocity ratio v_0/U is obtained by doing the weighted average of the values of v_0/U at the three vertices of the triangle (23). The weights are the ratio between the area of the subtriangle formed by the projected point and two vertices of the triangle and the area of the entire triangle.

Results

Validation of the method for an ovalbumin capsule

By way of illustration, we estimate the values of Ca, a/ℓ and v_o/U for the ovalbumin microcapsule depicted in the middle of Fig. 3a. The input geometrical quantities required by the method are the ones measured using the software *ImageJ*: $L_z/\ell = 2.14$ and $L_a/\ell = 1.81$. The resulting output values provided by the inverse analysis method are $Ca = 0.082$, $a/\ell = 0.96$ and $v_o/U = 1.29$. Since this case was not part of the database, we deduce the corresponding numerical contour by weight-averaging the contours of the $N = 14$ neighbors. The superposition of the experimental image with the estimated numerical contour is shown Fig. 3b. The very good qualitative correspondence of the measured and predicted capsule profiles is consolidated by the mean distance between both sets of points (i.e. the Hausdorff Distance normalized by a), which presently is 0.066. This validates the use of the diffuse approximation method for mechanical identification.

Error estimation in the entire parameter space

An algorithm has been designed to assess the accuracy of the solutions $\boldsymbol{\theta}$ provided by the method. A series of M test sets $\mathcal{L}_i^*$, for $i = 1, \ldots, 137$, has been generated in such a way that $\mathcal{L}_i^* = \mathcal{L} - \{\boldsymbol{\lambda}^i\}$. For each test set $\mathcal{L}_i^*$, we thus remove a point $\boldsymbol{\lambda}^i$ that emulates an experimental result. By applying the described method, $\boldsymbol{\theta} = (Ca, a/\ell, v_o/U)$ is obtained. It is expected to have the same value as $\boldsymbol{\theta}^i \in \mathcal{T}$. The relative errors between $\boldsymbol{\theta}$ and $\boldsymbol{\theta}^i$ are computed as

$$\varepsilon_j^i = \frac{\left|\theta_j - \theta_j^i\right|}{\theta_j^i},$$

with $j = 1, 2, 3$.

An overview of the resulting relative errors is provided for each parameter in Fig. 11 by heat maps. The errors are

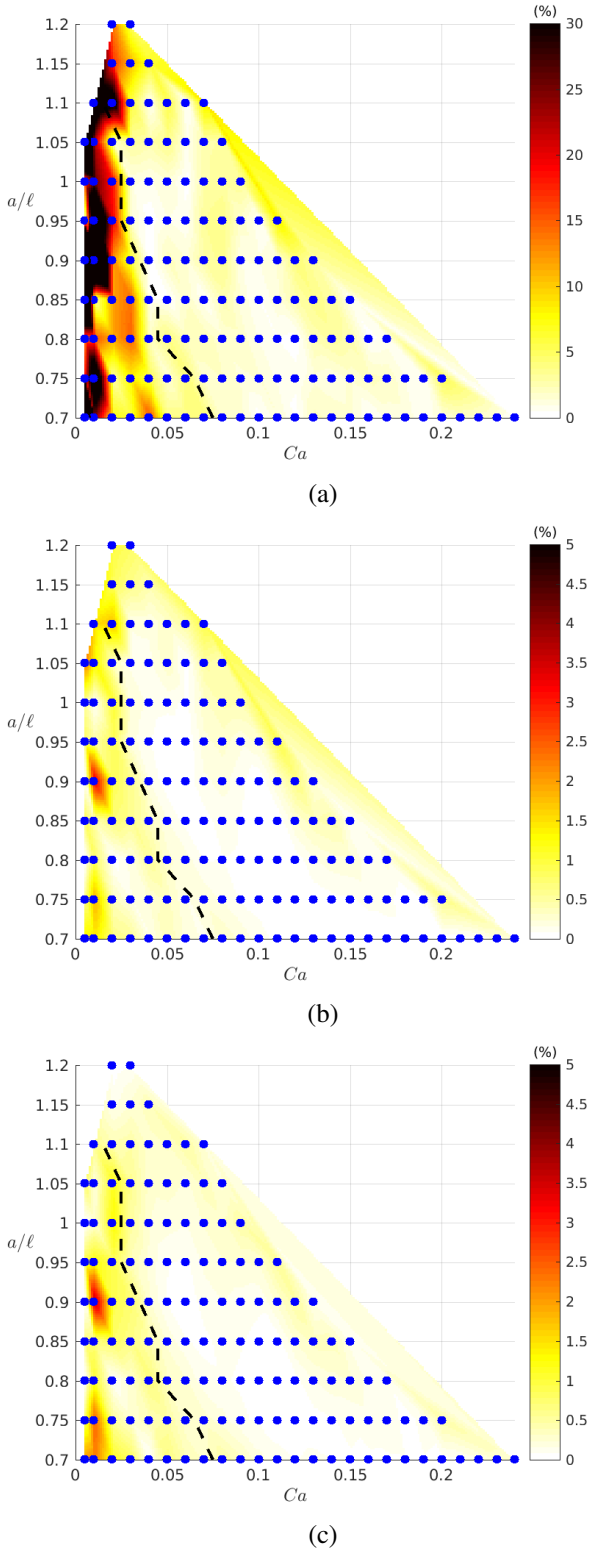

Figure 11. Heat maps of the relative errors ε, as a function of Ca and a/ℓ, when estimating (a) Ca, (b) a/ℓ and (c) v_o/U. The region to the left of the dashed black line indicates capsule stretch ratios $\Lambda \leq 1.04$.

generally higher along the borders of the domain than in the central region, especially for Ca. Previous studies showed that the identification method is only robust for sufficiently deformed capsules (10; 20). They based the criterion of reliability of the method on a global capsule stretch ratio $\Lambda = P/2\pi a$, P being the perimeter of the deformed capsule profile and $2\pi a$ the capsule perimeter at rest. They choose $\Lambda > 1.04$ as criterion (dashed black line in Fig 11).

If we only consider the cases that respect the criterion, we find mean relative errors equal to $\bar{\varepsilon}_1 = 2.7\% \pm 4.1\%$ for Ca, $\bar{\varepsilon}_2 = 0.2\% \pm 0.1\%$ for a/l, and $\bar{\varepsilon}_3 = 0.2\% \pm 0.2\%$ for v_o/U (despite the notations, one must note that the errors cannot be negative). We thus find that the errors are ten times smaller on a/ℓ and v_o/U than on Ca.

Discussion

The high correspondence between the capsule contour measured experimentally and that identified from the numerical simulation using diffuse approximation (e. g. Fig. 3b) indicates that it is a very efficient technique to identify the mechanical properties of micrometric deformable capsules.

The mean error values indicate that the method is able to retrieve the unknown values of the microcapsule size a (from a/l) and mean flow velocity U (from v_o/U) with a precision well below 1%. As for the value of the surface shear modulus G_S of the very thin microcapsule membrane, it is determined with a precision below 3%, which is remarkable for such small objects. The final precision on the determination of G_S will additionally depend on the precision of the measurement of the viscosity μ of the suspending fluid, which is likely to be within a few percent (20).

The present results provide very interesting insight on the limit of the microchannel identification method. They show that the reliability criterion based on the global capsule stretch ratio Λ is very relevant. The advantage is that Λ is a quantity that can be determined from the images acquired experimentally and can thus provide an indication on the level of deformation of the microcapsule membrane. The limiting value was defined as $\Lambda = 1.03$ for Hu et al. (10), which was corrected to $\Lambda = 1.04$ by Gubspun, Gires et al (20). Fig. 11, on which the lines $\Lambda = 1.04$ have been added for indication, shows that a good accuracy is reached even for confinement ratios $0.70 \leq a/l \leq 0.85$. No such results were obtained in the previous studies, because the microcapsules are too little deformed in the range. The diffuse approximation method thus allows to greatly extend the domain of validity of identification.

There is only one zone where the identification method leads to high errors even though the criterion is satisfied: $a/\ell \geq 1.1$ and $Ca \leq 0.03$. It is firstly caused by the intrinsic very low value of the capillary number in this region: small variations in the estimation of Ca lead to greater relative errors, especially in the Ca-range $[0.005, 0.04]$. Another cause is the abrupt changes in capsule deformed shapes that may happen for small increments of Ca when it is smaller than 0.02. Indeed, the capsule may not have a parachute shape ($L_p = 0$) for the very small values of Ca. The large elliptical neighborhood (with $N = 14$) thus contains the two kinds of deformed capsule profiles, some with a parachute and others without, which greatly impairs the identification precision.

When compared to previously developed inverse analysis procedures based on microfluidics (9; 10), much lower errors are currently found with the diffuse approximation technique. As soon as the capsule is sufficiently deformed,

the capsule size and surface shear modulus are determined with an error of only 0.2% and 2.7%, respectively. Hu *et al.* (10) detemined these quantities with an error of 2-3% and 25% in the best cases. Similar precision on the determination of mechanical properties was found using micropipette aspiration. Zhelev *et al.* (24), for instance, estimated the error to be within 25%. Using diffuse approximation for identification thus improves both the accuracy and reliability of the results.

The present results have been obtained for the neo-Hookean law, since we were interested in applying the technique to characterize the mechanical properties of ovalbumin capsules. The method is, however, valid regardless of the constitutive law used and could be applied to any artificial or natural (micro)capsule. The only challenge to use it on cells such as the red blood cells is purely experimental: the cells will indeed have to be flowed in a microchannel of about 10 microns. The results will have to be analyzed using the numerical database obtained for the Skalak's law (10), which has been shown to well model their membrane deformation (25).

Conclusion

We have presented a novel inverse analysis procedure that uses a data-driven diffuse approximation technique to identify the mechanical properties of microcapsule populations. This procedure is applied to the flow of a capsule through a long prismatic microfluidic channel of comparable size. The hydrodynamic forces inside the channel lead to the deformation of the membrane of the capsule, which eventually reaches a steady-state shape. The latter depends on the constitutive law of the membrane and two independent parameters: the capillary number Ca and the size ratio a/ℓ. Geometrical quantities characterizing the capsule deformed profiles at steady state are determined from the images acquired experimentally using a rapid camera mounted on a microscope.

The identification method is based on the results of numerical simulations of the fluid-structure interactions between the capsule wall and the fluid flows, obtained off-line. A comprehensive database of microcapsule deformed profiles and velocity ratios v_o/U has been generated with the BI–FE numerical model described in (13) for different values of Ca and a/ℓ. Diffuse approximation uses this database to efficiently estimate the unknown values of Ca, a/ℓ and v_o/U of each capsule from its characteristic geometrical quantities measured experimentally. Low errors are achieved over a wide range of values of the estimated parameters, which indicates that the method allows to determine the surface shear modulus G_S of the microcapsule membrane with a precision below 3%. It opens interesting perspectives for industrial applications that rely on microcapsules to transport active material, and require a tight control of the capsule mechanical properties to secure the targeted delivery.

Conflicts of Interest

The authors certify that they have no conflict of interest.

References

[1] Barthès-Biesel D. Motion and deformation of elastic capsules and vesicles in flow. Annu Rev Fluid Mech 2016; 48: 25–52.

[2] Ma G and Su Z. Microspheres and Microcapsules in Biotechnology: Design, Preparation and Applications. CRC Press, 2013.

[3] Yih TC and Al-Fandi M. Engineered nanoparticles as precise drug delivery systems. J Cell Biochem 2006; 97(6): 1184–1190.

[4] Nelson G. Application of microencapsulation in textiles. Int J Pharm 2002; 242(1): 55–62.

[5] Miyazawa K, Yajima I, Kaneda I et al. Preparation of a new soft capsule for cosmetics. J Soc Cosmet Chem 2000; 51(4): 239–252.

[6] Gibbs BF, Kermasha S, Alli I et al. Encapsulation in the food industry: a review. Int J Food Sci Nutr 1999; 50(3): 213–224.

[7] Needham D and Zhelev DV. The mechanochemistry of lipid vesicles examined by micropipet manipulation techniques. Surfactant Sci Ser 1996; 62: 373–444.

[8] Fery A and Weinkamer R. Mechanical properties of micro- and nanocapsules: Single-capsule measurements. Polymer 2007; 48(25): 7221–7235.

[9] Chu TX, Salsac AV, Leclerc E et al. Comparison between measurements of elasticity and free amino group content of ovalbumin microcapsule membranes: discrimination of the cross-linking degree. J Colloid Interface Sci 2011; 355(1): 81–88.

[10] Hu XQ, Sévénié B, Salsac AV et al. Characterizing the membrane properties of capsules flowing in a square-section microfluidic channel: Effects of the membrane constitutive law. Phys Rev E 2013; 87(6): 063008.

[11] De Loubens C, Deschamps J, Georgelin M et al. Mechanical characterization of cross-linked serum albumin microcapsules. Soft Matter 2014; 10: 4561–4568.

[12] Lefebvre Y and Barthès-Biesel D. Motion of a capsule in a cylindrical tube: effect of membrane pre-stress. J Fluid Mech 2007; 589: 157–181.

[13] Hu XQ, Salsac AV and Barthès-Biesel D. Flow of a spherical capsule in a pore with circular or square cross-section. J Fluid Mech 2012; 705: 176–194.

[14] Lac E, Barthès-Biesel D, Pelekasis NA et al. Spherical capsules in three-dimensional unbounded Stokes flows: effect of the membrane constitutive law and onset of buckling. J Fluid Mech 2004; 516: 303–334.

[15] Nayroles B, Touzot G and Villon P. Generalizing the finite element method: diffuse approximation and diffuse elements. Comput Mech 1992; 10(5): 307–318.

[16] Kuriakose S and Dimitrakopoulos P. Motion of an elastic capsule in a square microfluidic channel. Phys Rev E 2011; 84(1): 011906.

[17] Edwards-Lévy F, Andry MC and Lévy MC. Determination of free amino group content of serum albumin microcapsules using trinitrobenzenesulfonic acid: effect of variations in polycondensation pH. Int J Pharm 1993; 96(1-3): 85–90.

[18] McDonald JC and Whitesides GM. Poly(dimethylsiloxane) as a material for fabricating microfluidic devices. Acc Chem Res 2002; 35(7): 491–499.

[19] Fiorini G and Chiu D. Disposable microfluidic devices: fabrication, function, and application. BioTechniques 2005;

38(3): 429–450.

[20] Gubspun J, Gires PY, De Loubens C et al. Characterization of the mechanical properties of cross-linked serum albumin microcapsules: effect of size and protein concentration. Colloid Polym Sci 2016; 294(8): 1381–1389.

[21] Barthès-Biesel D. Modeling the motion of capsules in flow. Curr Opin Colloid Interface Sci 2011; 16(1): 3–12.

[22] Meng L, Breitkopf P, Le Quilliec G et al. Nonlinear shape-manifold learning approach: concepts, tools and applications. Arch Comput Method Eng 2018; 25: 1–21.

[23] Amidror I. Scattered data interpolation methods for electronic imaging systems: a survey. Journal of Electronic Imaging 2002; 11(2): 157. DOI:10.1117/1.1455013.

[24] Zhelev DV, Needham D and Hochmuth RM. A novel micropipet method for measuring the bending modulus of vesicle membranes. Biophysical Journal 1994; 67: 720–727.

[25] Skalak R, Tozeren A, Zarda RP et al. Strain energy function of red blood cell membranes. Biophys J 1973; 13(3): 245–264.

Acknowledgements

This work was supported by the Labex MS2T through the program "*Investments for the future*" funded by the French Government and managed by the National Agency for Research (Reference ANR-11-IDEX-0004-02). This project also received funding from the European Research Council (ERC) under the European Union's Horizon 2020 research and innovation programme (Grant agreement No. ERC-2017-COG - MultiphysMicroCaps)".